

# Natural convection for anomalous density variation of water: numerical benchmark

**T. Michalek\* and T.A. Kowalewski**

Department of Mechanics and Physics of Fluids,  
Institute of Fundamental Technological Research,  
Polish Academy of Sciences, Warsaw 00-049, Swietokrzyska 21, Poland  
E-mail: tmichal@ippt.gov.pl      E-mail: tkowale@ippt.gov.pl

\*Corresponding author

**B. Šarler**

Nova Gorica Polytechnic, Laboratory for Multiphase Processes,  
SI-5000 Nova Gorica, Vipavska 13, Slovenia  
E-mail: bozidar.sarler@p-ng.si

**Abstract:** A steady-state natural convection in a differentially heated cavity for temperatures in a vicinity of the freezing point is used to investigate and compare performance of four different numerical methods: finite differences, finite volume, finite elements and mesh-free diffuse approximation method. A primary aim of the exercise is to define a new numerical benchmark solution for natural convection problems, which includes challenging configuration of strongly non-linear buoyancy term. This configuration is used to test the performance of two popular commercial codes (Fluent and Fidap) and to compare them with two 'classical' finite difference codes and the new promising mesh-free implementation.

**Keywords:** numerical simulation; numerical benchmarks; mesh-free methods; natural convection.

**Reference** to this paper should be made as follows: Michalek, T., Kowalewski, T.A. and Šarler, B. (2005) 'Natural convection for anomalous density variation of water: numerical benchmark', *Progress in Computational Fluid Dynamics*, Vol. 5, Nos. 3/4/5, pp.158–170.

**Biographical notes:** Tomasz Michalek received a MSc degree in Computer Science from Jagiellonian University, Cracow, Poland in 1999. He is working toward the PhD degree in mechanics and physics of fluids at the Polish Academy of Sciences, Warsaw, Poland. His research interests include numerical methods, computational fluid dynamics, experimental and numerical benchmarking, object oriented programming and bioinformatics.

Tomasz A. Kowalewski received a MSc degree in Physics from Warsaw University in 1969 and a PhD in Fluid Dynamics from the Polish Academy of Sciences in 1982. Currently, he is associate professor and head of the department of Mechanics and Physics of Fluids at the Institute of Fundamental Technological Research at the Polish Academy of Sciences. His research interests include low Reynolds number flow of suspensions, modelling of the fibre spinning, experimental and numerical investigation of natural convection, particle image velocimetry and thermometry, computational and experimental fluid dynamics.

Božidar Šarler received a MSc degree in Industrial Physics from the University of Ljubljana in 1982 and a PhD in Mechanical Engineering from the University of Maribor in 1991. Currently, he is associate professor and head of Laboratory for Multiphase Processes at the Nova Gorica Polytechnic. His research interests include development of mesh reduction numerical techniques for transport phenomena, Stefan problems, porous media flow, and development of industrial simulation systems for continuous casting of steel and aluminium alloys.

---

## 1 INTRODUCTION

---

Natural convection flow in enclosures and cavities has received considerable attention in the recent heat transfer studies, largely due to its direct relevance in a variety of applications, ranging from growth of crystals, energy storage, spread of pollution to large-scale phenomena in foundry industry or environmental flows that influence important issues such as migration of pollutants in soil. Mathematical models describing natural convection involve a basic set of convection–diffusion equations used in fluid mechanics, namely the Navier-Stokes equations coupled with the energy transport equation. Therefore, the natural convection is also frequently selected as a standard configuration to verify correctness and performance of numerical schemes used in the computational fluid dynamics. De Vahl Davis [1] defined the most common reference solution over 20 years ago. It describes steady-state natural convection of a low Prandtl number ( $Pr = 0.71$ ) Boussinesq fluid in a differentially heated square cavity, with two isothermal and two adiabatic walls. Simplicity of the geometry combined with simple physics is the main advantage of the model. However, it appears that flow and temperature fields obtained for this configuration are quite smooth and even first-order solutions appear to be well performing, despite known limitations of such approach. In addition, it is difficult to validate obtained solutions, because it is impossible to build an experimental setup fulfilling adiabatic or at least nearly adiabatic thermal boundary conditions for air as a flow medium. Any solid material used for the walls is a better conductor of heat than the media itself.

The aim of this work is to propose slightly modified configuration of the de Vahl Davis benchmark, and to use it for testing performance of two commercial and two academic numerical codes. The proposed benchmark configuration concerns steady-state natural convection of water in the differentially heated square cavity. By setting the temperature range of isothermal walls close to the freezing point ( $T_h = 10^\circ\text{C}$ ,  $T_c = 0^\circ\text{C}$ ) and by adopting nonlinear variation of the water density with temperature a challenging flow configuration with two counter-rotating re-circulation zones is obtained. The competing effects of positive and negative buoyancy force, and interacting layers of hot and cold liquid, create interesting and difficult to model flow pattern. The two circulations create nearly vertical stratification, separating fluid in the cavity into two regions separated by the density maximum. An interesting configuration for studying heat transfer in a thin, well defined mixing zone separating hot and cold region of the same fluid is obtained. The hot and cold flow streams collide in the vicinity of the cold wall creating stagnation point, region of high velocity gradients. The position of the stagnation point appears to be an easy to monitor and very sensitive parameter revealing changes of the flow structure, favourable for detecting changes in experimental conditions or inaccuracies of numerical solutions.

Water is an important flow media for many practical and environmental flows. It has well know physical properties and high thermal conductivity, hence experimental validations can be relatively easily performed [2,3]. Natural convection of water in the vicinity of the freezing point has been used as an initial condition for the freezing experiments and numerical modelling of solidification process [3]. It is therefore very important to obtain trustful initial solutions, before any phase change source terms are included in the numerical models.

Due to the anomaly of water density variation, the configuration does not allow for a simple scaling using non-dimensional parameters. Multiple semi-similar solutions preserving main flow configuration can be obtained by increasing the size of the cavity only. This can be easily done both numerically and experimentally. Presently, we limit ourselves to a single configuration, assuming the box size to be equal to 38 mm. This configuration has been intensively investigated experimentally in our laboratory in the past and used to validate numerical codes.

In the following we give numerical results obtained for this configuration with two commercial codes, finite volume code Fluent [4] and finite element code Fidap [5], and compare them with the reference finite difference approximation code FRECON3V [6], being a revised, variable properties version of the classical Frecon [1]. Finally performance of the new mesh-free numerical approach based on the diffuse approximation method is investigated and compared with the defined benchmark solutions. For the sake of completeness of the most frequently used numerical methodologies, we present numerical results obtained using our finite difference, vorticity – streamfunction code SOLVSTR.

---

## 2 PROBLEM FORMULATION

---

We consider a steady-state, two-dimensional natural convection of water in the differentially heated square cavity of a height  $L = 38$  mm. Two vertical walls are isothermal, kept at temperatures  $T_H = 10^\circ\text{C}$ ,  $T_C = 0^\circ\text{C}$ . Top and bottom walls are assumed to be adiabatic. In the physical experiment [3] the cavity is a Plexiglas cube and the isothermal walls are made of metal and kept at constant temperature by two powerful thermostats. Air surrounding cavity and finite thermal conductivity of the Plexiglas walls modify thermal boundary conditions. This effect has been discussed in the previous papers by Kowalewski and Rebow [3], Leonardi et al. [6], Giangi et al. [7] and should be included in the numerical code if the code validation is performed.

Natural convection in the cavity characterises variation of the temperature in the range of  $\Delta T = 10^\circ\text{C}$ . Hence, for any physical fluid also variation of its physical properties in space is inevitable. For example the viscosity of water increases by almost 20% at the cold wall. Giangi et al. [7] investigated the effect of the variation of

viscosity, thermal conductivity and thermal capacity of fluid on the flow pattern for the same flow configuration. The results indicated that whereas the thermal conductivity and the thermal capacity of water can be assumed constant for the small temperature variations present, the effect of viscosity variation is noticeable and should be taken into account when performing the code validation procedure.

In the present study we assume that investigated configuration has been already validated [2,8] and for simplicity limit ourselves to a simplified case, assuming adiabatic top and bottom walls and constant fluid properties. Our main aim is to verify performance of the numerical models and to estimate the accuracy of the discrete approximate solutions in the presence of strong velocity and temperature gradients generated by the nonlinear buoyancy term.

The basic equations describing the flow driven by natural convection consist of conservation of mass, momentum and energy, and are given by:

$$\frac{\partial u}{\partial x} + \frac{\partial w}{\partial y} = 0 \quad (1)$$

$$\rho_0 \frac{\partial u}{\partial t} + \rho_0 u \frac{\partial u}{\partial x} + \rho_0 w \frac{\partial u}{\partial y} = -\frac{\partial p}{\partial x} + \mu \Delta u \quad (2)$$

$$\rho_0 \frac{\partial w}{\partial t} + \rho_0 u \frac{\partial w}{\partial x} + \rho_0 w \frac{\partial w}{\partial y} = -\frac{\partial p}{\partial y} + \mu \Delta w - g[\rho(T) - \rho_0] \quad (3)$$

$$\frac{\partial T}{\partial t} + u \frac{\partial T}{\partial x} + w \frac{\partial T}{\partial y} = \alpha \Delta T \quad (4)$$

The above equations describe the two-dimensional flow of an incompressible viscous fluid, where  $u$ ,  $w$ ,  $\rho_0$ ,  $p$ ,  $\mu$ ,  $g$ ,  $T$ ,  $\alpha$  denote, respectively, the horizontal and the vertical velocity, the reference density of fluid, the pressure, the dynamic viscosity, the gravitational acceleration, the temperature and the thermal diffusivity. Physical properties of water like dynamic viscosity, specific heat, thermal conductivity and density are assumed constant and their value at the reference temperature  $T_{\text{ref}} = 0^\circ\text{C}$  is used. The values applied to the numerical models are collected in Table 1. The anomalous thermal variation of the water density is implemented in buoyancy term only (equation (3)). The fourth order polynomial

$$\begin{aligned} \rho(T) = & 999.840281167108 + 0.0673268037314653 \\ & \times T - 0.00894484552601798 \times T^2 + \\ & + 8.78462866500416 \times 10^{-5} \times T^3 \\ & - 6.62139792627547 \times 10^{-7} \times T^4, \end{aligned} \quad (5)$$

given previously by Kowalewski and Rebow [3] was used to describe variation of water density with temperature.

**Table 1** Physical properties of water used in the simulations

Material properties of water at $0^\circ\text{C}$		Value	Unit
$\rho_0$	density of water at reference temperature	999.8	$\text{kg/m}^3$
$\mu$	dynamic viscosity	0.0017888	$\text{kg/ms}$
$\kappa$	thermal conductivity	0.566	$\text{W/mK}$
$c_p$	specific heat	4212.0	$\text{J/kgK}$
$g$	gravitational acceleration	9.81	$\text{m/s}^2$
$\beta_0$	thermal expansion coefficient	-6.733353E-05	$1/\text{K}$

Thermal boundary conditions for isothermal walls were taken  $T_h = 10^\circ\text{C}$  for the hot, and  $T_c = 0^\circ\text{C}$  for the cold wall, respectively. For the adiabatic walls the zero heat flux thermal boundary condition is set. The standard no-slip boundary conditions at all walls are adopted for the velocity components. Dimension of the cavity  $L$  was 38 mm. A steady-state solution is searched for. Hence, the initial conditions play a secondary role and were not investigated. In most cases a uniform temperature of the fluid and zero velocity was assumed as an initial condition.

The Rayleigh (Ra) and Prandtl (Pr) numbers describing investigated configuration are based on the fluid properties taken at the reference temperature and the cavity height. Their values are:

$$\text{Ra} = \frac{g\beta\Delta TH^3}{\alpha\nu} = 1.503 \times 10^6,$$

$$\text{Pr} = \frac{\nu}{\alpha} = 13.31$$

Dimensionless variables are used in most of the codes. Hence, results of the tests are given in non-dimensional form using for non-dimensional temperature  $\vartheta$ , horizontal and vertical coordinates  $X$ ,  $Y$ , and horizontal and vertical velocities  $U$ ,  $W$  the following scales:

$$\begin{aligned} \vartheta = (T - T_c)/(T_h - T_c), \quad X = x/L, \\ Y = y/L, \quad U = uL/\alpha, \quad W = wL/\alpha \end{aligned} \quad (6)$$

In what follows, the non-dimensional values are exclusively used.

### 3 NUMERICAL ALGORITHMS

As we have mentioned above, the five different numerical approaches were tested. The extensive mesh-sensitivity tests were performed for each of them and the result of the best performing algorithm is selected as a reference solution. We present a short description of each code below and give

hints gained during code testing. Selected results of tests are collected in tables below. For comparison values of the global velocity extremes and the average Nusselt number for the cold wall are given for each case in the first part of the tables. The velocity extremes at the two section: the mid-horizontal line ( $Y = 0.5$ ), the mid-vertical line ( $X = 0.5$ ) are given for both component in the second part of each table.

**3.1 Vorticity-vector potential finite difference code FRECON3V**

A modified version of the three-dimensional numerical code FRECON3V (FRE) has been used to obtain reference solutions and to perform several tests of the model. This finite difference false transient solver, developed at the University of New South Wales, uses vorticity-vector potential formulation of the Navier-Stokes and energy equations for steady, laminar flow of a viscous, incompressible fluid. Solutions were obtained for Cartesian coordinates on uniform meshes. Reliability and robustness of the code has been tested over many years and has been reported in numerous papers [9,10]. It is also the fastest solver from among all others tested in this paper.

The two-dimensional solutions were obtained using the code FRE with only five grid points for the channel depth, with slip kinematic boundary condition and adiabatic thermal boundary conditions for the side walls to eliminate

the flow components in the third direction. These 2D results, generated for the sequence of mesh resolutions from  $21 \times 21$  to  $301 \times 301$  are given in Table 2. The maximum and minimum of the two velocity components and the averaged Nusselt number for the cold wall are displayed as basic monitors of the code convergence performance. Additionally we present max/min values of the velocity components on horizontal and vertical mid-line. The solutions were assumed to converge when all residues of the equations imbalance were less than  $10^{-9}$ . A typical CPU time necessary to reach converged solution shows nearly cubic growth with a grid resolution and varies from 180 sec for FRE1 to  $3.6 \times 10^5$  sec for FRE7 case (all CPU times are scaled to PentiumHT 3 GHz processor with 2 GB memory).

Figure 1 shows the velocity and temperature fields obtained for the run FRE6 solution. Two main circulations are clearly visible: an upper clockwise circulation transporting hot liquid towards the top wall and back along the isotherm of the density extremum, and a lower counter-clockwise circulation within the cold wall region. At the cold wall, the descending hot liquid interacts with the rising cold liquid. This creates a distinct saddle point in the vicinity of the wall, approximately at about two-thirds of the cavity height. Position of the saddle point, given by the balance of competing positive and negative buoyancy forces, appears to be very sensitive to inaccuracies of the numerical solutions.

**Table 2(a)** FRECON3V mesh dependence test: global velocity extremes and Nusselt number at the cold wall

Run	Mesh	$U_{min}$	$U_{max}$	$W_{min}$	$W_{max}$	$N_c$
FRE1	$21 \times 21$	-141.9	101.4	-225.6	215.2	7.05
FRE2	$41 \times 41$	-156.1	101.1	-177.0	213.1	6.98
FRE3	$81 \times 81$	-158.7	102.9	-175.7	217.3	6.60
FRE4	$121 \times 121$	-158.8	103.1	-175.8	221.4	6.52
FRE5	$161 \times 161$	-159.1	103.3	-175.9	222.0	6.49
FRE6	$201 \times 201$	-159.2	103.3	-175.9	221.9	6.48
FRE7	$301 \times 301$	-159.2	103.4	-176.0	222.5	6.47

**Table 2(b)** FRECON3V mesh dependence test: velocity extremes and their location for  $X = 0.5$  and  $Y = 0.5$

Run	Horizontal line $Y = 0.5$				Vertical line $X = 0.5$			
	$U_{min}/X$	$U_{max}/X$	$W_{min}/X$	$W_{max}/X$	$U_{min}/Y$	$U_{max}/Y$	$W_{min}/Y$	$W_{max}/Y$
FRE1	-103.0/0.80	20.4/0.55	-211.0/0.80	215.0/0.05	-96.6/0.15	82.0/0.90	0.75/0.95	9.72/0.30
FRE2	-132.0/0.72	6.25/0.42	-174.0/0.72	209.0/0.05	-75.4/0.25	84.2/0.90	-68.9/0.25	5.54/0.60
FRE3	-131.0/0.71	3.65/0.39	-174.0/0.71	213.0/0.04	-76.8/0.28	86.0/0.89	-84.5/0.26	6.28/0.64
FRE4	-131.0/0.71	3.21/0.38	-175.0/0.71	216.0/0.04	-77.4/0.28	86.5/0.89	-86.6/0.26	6.40/0.65
FRE5	-131.0/0.71	3.06/0.38	-175.0/0.70	216.0/0.04	-77.6/0.29	86.6/0.89	-87.2/0.26	6.44/0.65
FRE6	-131.0/0.71	3.00/0.38	-175.0/0.70	216.0/0.04	-77.7/0.29	86.6/0.89	-87.5/0.26	6.46/0.65
FRE7	-131.0/0.71	2.94/0.38	-175.0/0.70	217.0/0.04	-77.8/0.29	86.7/0.89	-87.7/0.26	6.48/0.65

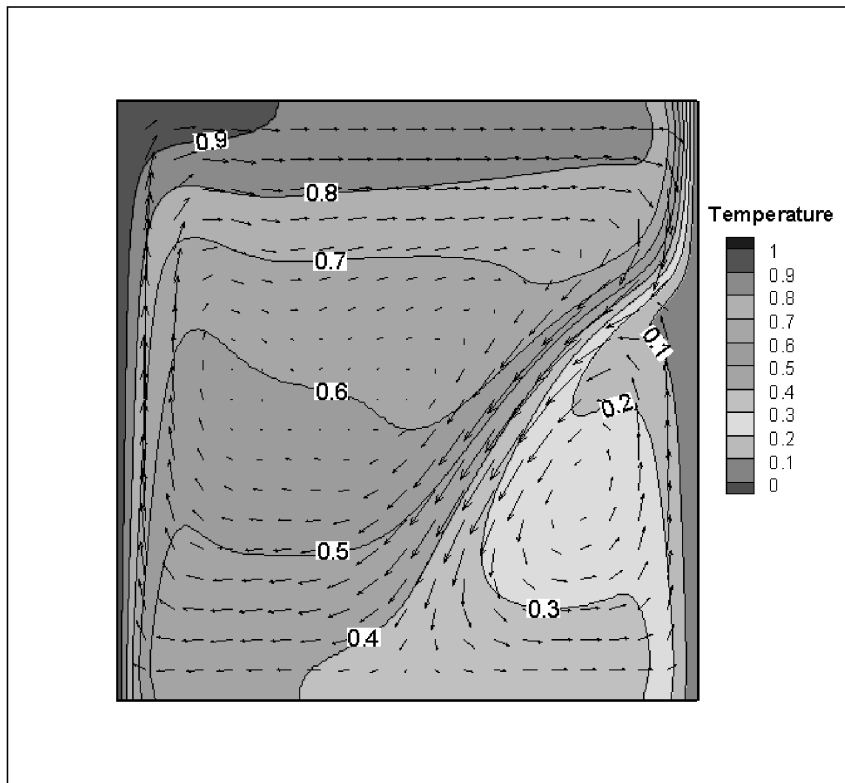


**Figure 1** Natural convection of water. Temperature and velocity field for the fine mesh solution of FRECON3V (run FRE6)

### 3.2 Finite volume code FLUENT

A steady-state two-dimensional solutions for the problem defined above were obtained using commercial finite volume code Fluent 6.2 [4]. Several uniform structural grids were tested, results obtained for four of them are displayed in Table 3. Fluent gives possibility to select large spectrum of different solvers and solving strategies using the user friendly interface. Selection of the appropriate model is often crucial both in terms of speed as well as accuracy of the result. Following experience gained during several test runs the implicit false transient method was used to reach efficiently a steady state. Spatial derivatives were approximated using QUICK scheme, which is based on a weighted average of second-order-upwind and central interpolation of the variable. Pressure-velocity coupling was done using SIMPLE algorithm. The nonlinear density variation given by equation (5) was implemented in the solver. Fluent uses internally dimensional variables, hence results of the simulations were scaled using relations (6). The convergence criteria was given by the residua of the solution less than  $10^{-6}$ . It turned out that solutions obtained using single precision solver were different by more than 5% for extremes of velocity values and their location, even for the finest mesh  $380 \times 380$ . Therefore, all the results reported in this work were performed using double precision solver. A typical CPU time necessary to reach converged solution for the coarse mesh case (FLU0) is  $2 \times 10^4$  s, which is much slower in comparison with the FRECON solver. It is worth noting,

however, that solution obtained for this relative coarse mesh is much closer to the fine mesh solution (FRE7) than a similar solution obtained with the FRECON (FRE2).

### 3.3 Finite element code FIDAP

A steady-state two-dimensional solution for the problem defined above were obtained using commercial, finite element method code Fidap 8.7. The quadrilateral elements and bilinear shape functions were used to discretise the computational domain. The non-linear system of matrix equations arising from the FEM discretisation is solved separately in sequential manner using so called segregated solver [5]. The non-linear density variation given by (5) was implemented in the solver. Fidap similar to Fluent uses internally dimensional variables, hence results of the simulations were scaled appropriately. The convergence criteria was given by the residua of the solution less than  $10^{-4}$ . Fidap appears to be a very fast and stable solver, producing reasonable results even for a coarse mesh. The global values of the solutions (Nusselt number, global velocity extremes) seem to match well with the fine mesh solutions obtained using other codes (e.g., FRE6). However, more detailed analysis reveals that solutions obtained with Fidap, even for the fine meshes, exhibit considerable errors when flow structure is compared (see Section 4). Table 4 collects results obtained for two different grid resolutions. It is worth noting that CPU time necessary to obtain the solutions is almost five times shorter than for a corresponding Fluent run.

**Table 3(a)** FLUENT mesh dependence test: global velocity extremes and Nusselt number at the cold wall

Run	Mesh	$U_{min}$	$U_{max}$	$W_{min}$	$W_{max}$	Nu
FLU0	38 × 38	-158.94	105.31	-172.38	208.12	6.59
FLU1	76 × 76	-159.39	103.57	-173.61	220.60	6.47
FLU2	190 × 190	-159.77	103.51	-174.57	223.21	6.51
FLU3	380 × 380	-159.73	103.55	-174.73	223.52	6.50

**Table 3(b)** FLUENT mesh dependence test: velocity extremes and their location for  $X = 0.5$  and  $Y = 0.5$

Run	Horizontal line $Y=0.5$				Vertical line $X=0.5$			
	$U_{min}/X$	$U_{max}/X$	$W_{min}/X$	$W_{max}/X$	$U_{min}/Y$	$U_{max}/Y$	$W_{min}/Y$	$W_{max}/Y$
FLU0	-136.04/0.71	2.46/0.39	-171.09/0.71	202.15/0.053	-80.35/0.29	88.92/0.89	-87.17/0.26	6.25/0.63
FLU1	-134.08/0.71	2.83/0.38	-172.41/0.71	215.36/0.039	-78.87/0.29	87.18/0.89	-87.90/0.26	6.39/0.64
FLU2	-132.72/0.71	2.92/0.38	-173.40/0.70	217.53/0.040	-78.22/0.28	86.90/0.89	-87.62/0.26	6.44/0.64
FLU3	-131.68/0.70	2.93/0.38	-173.62/0.70	217.84/0.042	-78.11/0.28	86.85/0.89	-87.37/0.26	6.42/0.64

**Table 4(a)** FIDAP mesh dependence test: global velocity extremes and Nusselt number at the cold wall

Run	Elements	$U_{min}$	$U_{max}$	$W_{min}$	$W_{max}$	Nu
FID1	39x39	-155.10	104.30	-178.07	227.02	6.64
FID2	77x77	-159.03	105.38	-174.93	225.17	6.44

**Table 4(b)** FIDAP mesh dependence test: velocity extremes and their location for  $X = 0.5$  and  $Y = 0.5$ .

Run	Horizontal line $Y = 0.5$				Vertical line $X = 0.5$			
	$U_{min}/X$	$U_{max}/X$	$W_{min}/X$	$W_{max}/X$	$U_{min}/Y$	$U_{max}/Y$	$W_{min}/Y$	$W_{max}/Y$
FID1	-130.47/0.71	4.36/0.39	-177.15/0.71	218.50/0.05	-77.05/0.29	94.14/0.92	-83.74/0.26	6.03/0.60
FID2	-131.50/0.70	5.28/0.38	-174.31/0.70	219.71/0.04	-81.60/0.29	87.57/0.89	-99.19/0.26	7.19/0.68

**3.4 Finite difference stream function – vorticity code SOLVSTR**

A classical two-dimensional stream function – vorticity  $\psi$ - $\zeta$  solver was applied to get steady-state two-dimensional solutions for the investigated model. An implicit false transient approach was applied to all equations. Discretisation of  $\psi$ - $\zeta$  and energy equations were done making use of second order central difference scheme in space. The equations were solved by an alternating direction implicit method (ADI) algorithm. The resulting algebraic

equations are tridiagonal and easily solved by TDMA algorithm. The approach used is comparable to the FRECON algorithm, it also performs relatively fast. Typical CPU time to reach converged solution (residuals  $< 10^{-9}$ ) is about  $10^5$  sec for  $200^2$  mesh. However, the convergence rate, what will be also visible further, is slow in comparison with other algorithms. Mesh dependence test indicates difficulties of the code to reach accurate solution, even for the finest mesh. It illustrates, similar to the above-mentioned Fidup solutions, that ‘grid-converged’ solution does not necessarily mean ‘true’ solution.

**Table 5(a)** SOLVSTR mesh dependence test: global velocity extremes and Nusselt number at the cold wall

Run	Mesh	$U_{min}$	$U_{max}$	$W_{min}$	$W_{max}$	Nu
STR1	50 × 50	-178.51	116.425	-191.450	248.063	6.63
STR2	100 × 100	-168.73	108.743	-183.605	237.538	6.78
STR3	150 × 150	-165.34	106.777	-180.327	232.612	6.73
STR4	200 × 200	-163.60	105.728	-179.554	229.670	6.67
STR5	250 × 250	-162.45	105.047	-177.356	227.635	6.65

**Table 5(b)** SOLVSTR mesh dependence test: velocity extremes and their location for  $X = 0.5$  and  $Y = 0.5$ 

Run	Horizontal line $Y = 0.5$				Vertical line $X = 0.5$			
	$U_{min}/X$	$U_{max}/X$	$W_{min}/X$	$W_{max}/X$	$U_{min}/Y$	$U_{max}/Y$	$W_{min}/Y$	$W_{max}/Y$
STR1	-147.20/0.67	1.15/0.37	-191.45/0.67	237.34/0.04	-95.57/0.31	96.26/0.90	-119.59/0.29	7.10/0.67
STR2	-139.71/0.71	2.43/0.37	-183.04/0.70	230.38/0.04	-84.74/0.28	90.93/0.89	-95.47/0.26	6.64/0.64
STR3	-137.10/0.70	2.61/0.38	-179.69/0.70	226.18/0.04	-82.09/0.28	89.38/0.89	-91.34/0.25	6.55/0.64
STR4	-135.64/0.71	2.68/0.38	-177.74/0.70	223.58/0.04	-80.78/0.28	88.54/0.89	-89.75/0.26	6.51/0.64
STR5	-134.14/0.71	2.44/0.38	-176.64/0.70	221.48/0.04	-79.62/0.28	87.96/0.89	-87.31/0.26	6.52/0.64

### 3.5 Mesh-free diffuse approximation method code SOLVMEF

Mesh-free methods allow to establish a system of algebraic equations for the whole problem domain without use of a predefined mesh. These methods do not use polygonisation of the domain and/or boundary. Instead, solution is generated in a set of nodes, similarly as in the finite difference method, however with great flexibility of positioning the calculation nodes. There is a plethora of the mesh-free methods proposed using different approaches and names, the methodology is still in a rapid development stage. The state-of-the-art of these methods can be found in recent books [11,12]. Their main advantage is large flexibility when applied to complex geometries, usually same formulation for 2D and 3D, easy node refinement, and ease of coding. Recently, some of these methods were successfully tested for the heat transfer CFD problems without [13] and with [14] phase change. The performance of one of the mesh-free methods was tested using proposed benchmark configuration. The Navier-Stokes equations in stream function–vorticity formulation were discretised making use of the diffuse approximation method (DAM). The diffuse approximation is a weighted least-squares approximation of a scalar field and its derivatives, and is closely related to the moving least-square method [15,16]. Generally, the method can be applied to any distribution of the collocation points. In the following, for simplicity, we assumed uniform distribution of collocation points inside the computational domain. Employing this assumption and selecting six simplest polynomial bases for the approximation  $(1, x, y, x^2, xy, y^2)$ , we come to the following analytical formulas (7–10) for the first and second derivatives. These derivatives are used to discretise stream function, vorticity and energy equations. For a scalar function  $\Phi$  the diffuse approximation of its first and second derivatives at the arbitrary point  $P$  are defined in the following way:

$$\frac{\partial \Phi}{\partial x} = \frac{w_1(\Phi_E - \Phi_W) + w_2(\Phi_{NE} - \Phi_{NW}) + w_2(\Phi_{SE} - \Phi_{SW})}{2hw_1 + 4hw_2} \quad (7)$$

$$\frac{\partial \Phi}{\partial y} = \frac{w_1(\Phi_N - \Phi_S) + w_2(\Phi_{NW} - \Phi_{SW}) + w_2(\Phi_{NE} - \Phi_{SE})}{2hw_1 + 4hw_2} \quad (8)$$

$$\frac{\partial^2 \Phi}{\partial x^2} = \frac{\Phi_E - 2\Phi_P + \Phi_W}{h^2} \quad \frac{\partial^2 \Phi}{\partial y^2} = \frac{\Phi_N - 2\Phi_P + \Phi_S}{h^2} \quad (9)$$

$$\frac{\partial^2 \Phi}{\partial x \partial y} = \frac{\Phi_{SW} + \Phi_{NE} - \Phi_{NW} - \Phi_{SE}}{4h^2} \quad (10)$$

where  $h$  stands for the distance between two neighbouring points (see Figure 2), and  $\Phi_P, \Phi_N, \Phi_S, \Phi_W, \Phi_E, \Phi_{NW}, \Phi_{NE}, \Phi_{SW}, \Phi_{SE}$  denote the values of a function being approximated in the vicinity of arbitrary point  $P$ ,  $w_1, w_2$  denote the value of a weighting function. In the present calculations the following weighting function is used:

$$\begin{cases} w(P, Z) = \exp\left[-\ln(10)\left(\frac{r}{h\sqrt{2}}\right)^2\right] & \text{if } r \leq h\sqrt{2} \\ w(P, Z) = 0 & r > h\sqrt{2} \end{cases} \quad (11)$$

where  $r$  is the distance between  $P$  and  $Z$ . ( $Z$  is one of the neighbouring points,  $w_1 = w(P, N) = w(P, S) = w(P, E) = w(P, W)$ ,  $w_2 = w(P, NE) = w(P, NW) = w(P, SE) = w(P, SW)$ ).

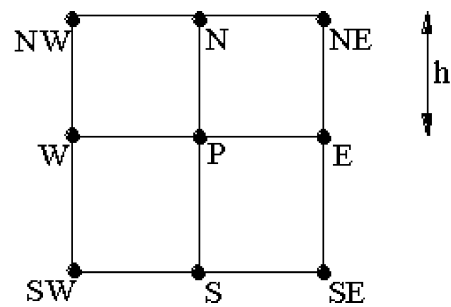


**Figure 2** Computational molecule used in the diffuse approximation method

The resulting algebraic equations result in a sparse matrix with at most nine non-zero elements in each row of a matrix, and are solved making use of Gauss-Seidel algorithm. The number of non-zero elements in the matrix is closely related to the number of neighbouring points taken into account during application of diffuse approximation.

Each computational molecule consists of nine nodes (see Figure 2). The use of Gauss-Seidel method to solve approximated equations makes the algorithm much slower in comparison with a classical approach, for instance the one applied in SOLVSTR. The application of much more sophisticated solvers will be considered in future work as

well as the use of a preconditioner to improve the performance of the algorithm. A CPU time necessary to reach converged solution (error less than  $10^{-6}$ ) for  $100^2$  mesh is fifteen times slower than the corresponding case performed by SOLVSTR algorithm. This made more extensive discretisation dependence study out of reach.

**Table 6(a)** SOLVMEF discretisation dependence test

Run	Number of points	$U_{min}$	$U_{max}$	$W_{min}$	$W_{max}$	$N_c$
MEF1	10000 ( $100 \times 100$ )	-161.87	103.78	-167.58	225.94	6.22

**Table 6(b)** SOLVMEF discretisation dependence test

Run	Horizontal line $Y = 0.5$				Vertical line $X = 0.5$			
	$U_{min}/X$	$U_{max}/X$	$W_{min}/X$	$W_{max}/X$	$U_{min}/Y$	$U_{max}/Y$	$W_{min}/Y$	$W_{max}/Y$
MEF1	-125.34/0.68	5.81/0.34	-166.91/0.64	218.89/0.04	-79.87/0.35	88.29/0.89	-132.03/0.31	6.56/0.71

**4 SELECTION OF THE REFERENCE SOLUTION**

In order to compare performance of different codes in terms of their ability to reproduce fine details of the flow structure it is not sufficient to verify agreement of global flow field parameters, like those given in Tables 2–6. It appears that small deviation in their value (2–5%) from the reference solution, usually reported as *reasonable* or even *excellent* agreement, corresponds to distinct changes of the flow pattern. Such changes become responsible for differences in the local mass and heat transfer in the system. These effects can perhaps be neglected if only insulation or heat drainage are of the main interest. But they are not tolerable when phase change processes are present (e.g., freezing of water) or transport of small inclusions is an important issue. For example if we compare Nusselt number of the most coarse solution FRE1 with that for a doubled mesh density (FRE2), one may get the impression that both solutions describe the same flow configuration. Comparison of the velocity profiles (Figure 3) clearly indicates that in fact these are two different flow fields. Hence, to obtain better insight into differences or similarities of the flow structures obtained from the investigated solvers, the second step of the verification procedure is proposed. It is based on calculating deviation of the velocity profiles extracted along three selected lines: horizontal centreline  $Y = 0.5$ , vertical centreline  $X = 0.5$  and vertical line passing through the mixing zone and the stagnation point at the cold wall ( $X = 0.9$ ). Locations of the lines are selected in such way that for any investigated mesh resolution they still match the nodes location, and additional interpolation errors are avoided. Figure 3 shows example of the velocity profiles along the horizontal and vertical symmetry lines of the cavity for meshes from Table 2. It is worth noting that the errors of the simulation performed for the quite fine mesh (FRE2) may reach almost 50% for the vertical velocity (Figure 3(a)). Also large errors are present for the horizontal velocity component obtained for the coarse mesh (Figure 3(b)). This test indicates that modelling of a simple natural convection in the presence of the strongly nonlinear

variation of water density requires careful analysis of results and very fine meshes.

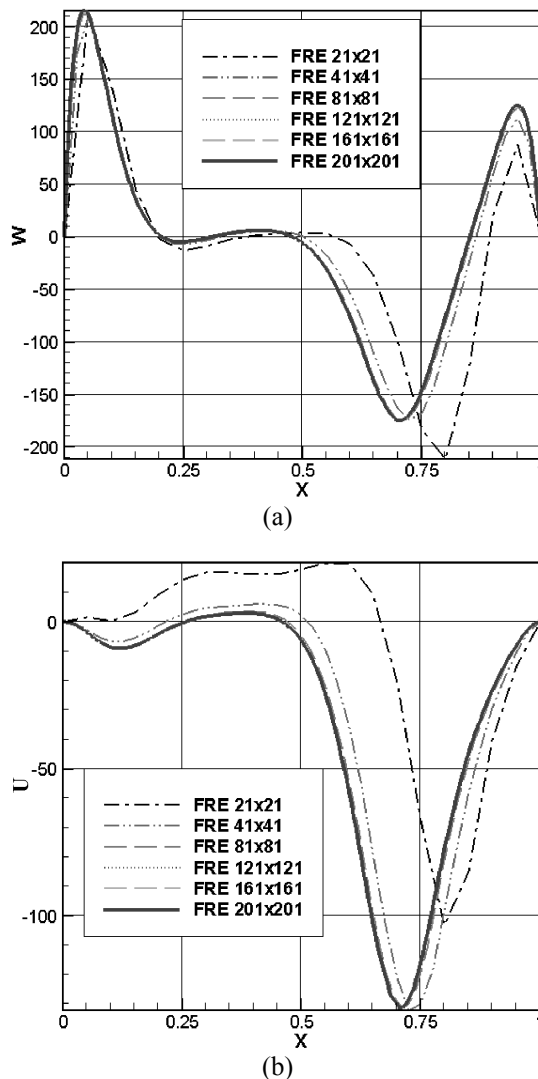


**Figure 3** Velocity profiles extracted for the horizontal centreline  $Y = 0.5$ ; (a) vertical velocity component, (b) horizontal velocity component

The mesh sensitivity analysis performed for five investigated codes gives us some reference about convergence rate and allows to estimate their asymptotic behaviour. For more detailed comparison the flow field obtained using FRECON3V for the fine mesh ( $201 \times 201$ ) was selected. The velocity and temperature profiles extracted along the above-mentioned lines are approximated with the high-order polynomial and treated as a reference (benchmark) solution. The numerical values of the polynomials coefficients are given in Appendix. The 15 digit accurate values of the coefficients are given to ease comparisons in the future. Obviously, it will be easier to quantify accuracy using well defined analytical functions than by overlapping reproduced figures.

An assessment on the accuracy of the solution is obtained calculating relative differences in terms of defined below standard deviations  $\sigma$ , evaluated for the polynomials describing benchmark profiles and corresponding values extracted from the interrogated solution:

$$\sigma = \frac{1}{N} \sum_{i=1}^N (f(x_i) - w(x_i))^2 \quad (12)$$

Here,  $N$  gives number of discrete points (corresponding to the discretisation nodes) of the interrogated solution,  $w(x_i)$  polynomial value of the benchmark solution for the point  $x_i$ , and  $f(x_i)$  value of the analysed discrete solution for the point  $x_i$ .

Nine indicators are defined according to the above definition and used to evaluate accuracy of the solutions:  $\sigma_{u1}$ ,  $\sigma_{w1}$ ,  $\sigma_{t1}$ ,  $\sigma_{u2}$ ,  $\sigma_{w2}$ ,  $\sigma_{t2}$ ,  $\sigma_{u3}$ ,  $\sigma_{w3}$  and  $\sigma_{t3}$ . They describe standard deviations calculated for two velocity components  $U$ ,  $W$  and temperature  $T$  for profiles extracted at centrelines  $Y=0.5$ ,  $X=0.5$ , and vertical line  $X=0.9$ .

The proposed accuracy indicators can be easily used to assess performance of any numerical solutions, regardless of dimension of the mesh size, as well as to estimate the rate of convergence of successive solutions. Data collected in Table 7 are presented in Figure 4. The figures show, respectively, mesh dependence of  $\sigma_{u1}$ ,  $\sigma_{w1}$  for velocity profiles at  $Y=0.5$ ,  $\sigma_{u2}$ ,  $\sigma_{w2}$  for velocity profiles at  $X=0.5$ ,  $\sigma_{u3}$ ,  $\sigma_{w3}$  for velocity profiles at  $X=0.9$ , and  $\sigma_{t1}$ ,  $\sigma_{t2}$ ,  $\sigma_{t3}$  for three temperature profiles at  $Y=0.5$ ,  $X=0.5$  and  $X=0.9$ .

**Table 7** Standard deviations from the reference solution (see Appendix) calculated for profiles of both velocity components and temperature obtained at the two mid-section ( $X=0.5$  and  $Y=0.5$ ) and close to the cold wall ( $X=0.9$ )

	Y = 0.5			X = 0.5			X = 0.9		
	$\sigma_{u1}$	$\sigma_{w1}$	$\sigma_{t1}$	$\sigma_{u2}$	$\sigma_{w2}$	$\sigma_{t2}$	$\sigma_{u3}$	$\sigma_{w3}$	$\sigma_{t3}$
FRE6	0.2831	1.3876	1.64E-06	0.1670	0.0024	8.03E-08	1.2667	0.6012	2.28E-05
FRE5	0.3284	1.6127	1.94E-06	0.2045	0.0293	2.14E-07	1.2213	0.6626	2.35E-05
FRE4	0.5411	1.8601	3.20E-06	0.4004	0.2127	8.77E-07	1.3658	0.9012	2.57E-05
FRE3	3.5512	7.7287	1.94E-05	2.4778	2.4683	8.55E-06	3.0392	4.3332	5.45E-05
FRE2	114.45	178.24	6.98E-04	69.645	95.363	2.48E-04	67.3915	144.683	1.10E-03
FRE1	1893.7	2857.7	4.40E-03	753.31	1874.6	1.36E-02	364.095	1492.25	9.50E-03
FLU3	1.5510	3.0529	5.32E-06	0.2201	0.0892	2.50E-06	4.8378	5.1385	7.08E-05
FLU2	1.8745	3.1868	6.84E-06	0.2514	0.0488	2.43E-06	5.3223	6.1924	7.79E-05
FLU1	6.1705	8.8068	4.52E-05	0.4913	0.2016	7.51E-08	34.2911	91.7224	3.68E-04
FLU0	28.760	49.564	3.55E-04	2.5880	1.2864	2.88E-05	91.4327	433.448	8.58E-04
FID2	3.8785	11.347	1.70E-05	7.7958	5.0095	1.48E-05	5.9907	18.3377	3.87E-05
FID1	10.678	24.737	6.03E-05	13.056	35.092	4.70E-05	15.0269	27.8671	2.04E-04
STR5	2.8876	10.924	8.17E-06	1.4492	1.1331	6.39E-06	7.0646	8.5051	7.10E-05
STR4	4.3005	18.850	8.95E-06	2.3089	1.2263	1.30E-05	11.1198	13.5929	8.40E-05
STR3	7.6570	34.860	1.87E-05	4.5268	2.9492	2.61E-05	16.8484	17.3370	9.09E-05
STR2	20.769	77.964	6.67E-05	11.768	11.837	5.88E-05	32.4156	20.6114	1.01E-04
STR1	283.48	506.50	1.26E-03	127.88	251.92	2.83E-04	221.818	79.4415	0.0014
MEF1	586.31	1176.3	3.48E-03	214.57	799.64	5.34E-04	267.977	481.019	0.0038

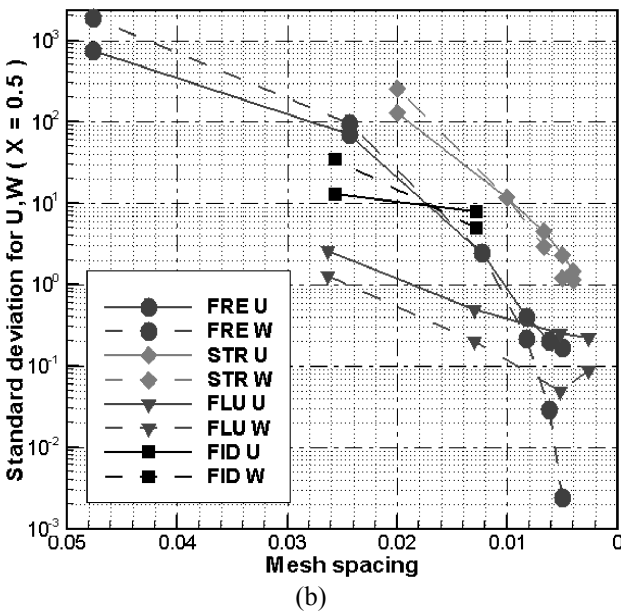
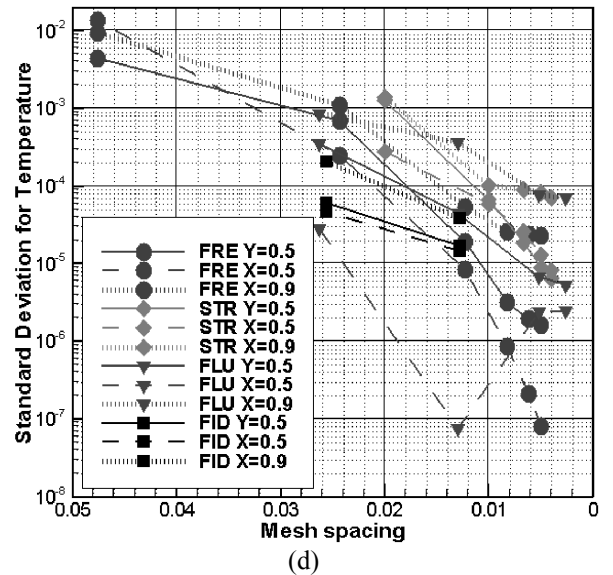
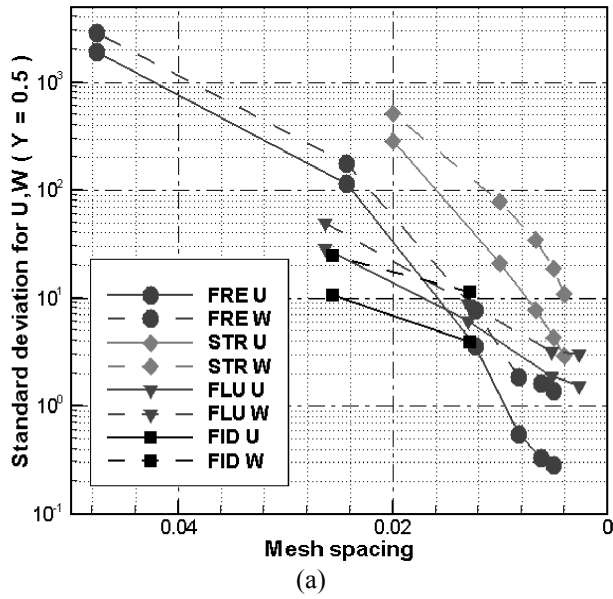
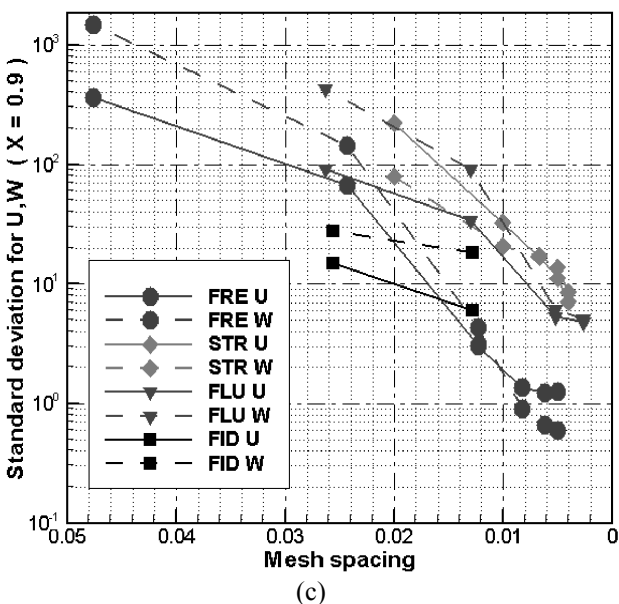


**Figure 4** Mesh dependence: (a) standard deviations  $\sigma_{v_1}, \sigma_{w_1}$  for velocity profiles at  $Y = 0.5$ , (b) standard deviations  $\sigma_{v_2}, \sigma_{w_2}$  for velocity profiles at  $X = 0.5$ , (c) standard deviations  $\sigma_{v_3}, \sigma_{w_3}$  for velocity profiles at  $X = 0.9$ , (d) standard deviations  $\sigma_{t_1}, \sigma_{t_2}, \sigma_{t_3}$  for three temperature profiles at and  $X = 0.9$



The value of  $\sigma_{u_1}, \sigma_{w_1}, \sigma_{u_2}, \sigma_{w_2}, \sigma_{u_3}, \sigma_{w_3}, \sigma_{t_1}, \sigma_{t_2}, \sigma_{t_3}$  for the fine mesh FRECON solution (FRE6) was taken as a reference error indicator. Generously setting cut-off value for standard deviation as equal to 3 we come to the conclusion that only solutions FRE4-7 and FLU3 are close enough to the reference solution to be assumed as the correct ones.

From Figure 4 it is easily visible that the rate of convergence of SOLVSTR is much slower in comparison with FRECON. On the other hand, analysing the values of the indicators on successive meshes we may find that the rate of convergence for FLUENT, FIDAP is almost linear in contrast to the much faster convergence of FRECON or even SOLVSTR. It is rather surprising as both the commercial codes claim to use second-order approximations.

The stream function–vorticity solver SOLVSTR needs almost triple mesh refining ( $250 \times 250$ ) to reach accuracy comparable with that of other ‘mesh related’ codes. One of the possible explanations of such behaviour is the lack of ‘upwind’ schemes in SOLVSTR code. Moreover, improvement of the ADI algorithm and replacement of Gauss-Seidel algorithm by relaxation methods like SOR, CG, GMRES, could lead to better performance of the code.

It is worth noting that convergence of temperature is relatively easy to reach, and even for the most coarse meshes temperature profiles are practically ‘exact’. It indicates robustness of the energy equations and relatively small effect of the convective term on the resulting temperature distribution. It is a rather surprising result, and it suggest that use of temperature as a convergence indicator can be dangerously misleading at least for the analysed flow configuration.

A mesh-free code MEF using diffuse approximation fails this very sensitive test of accuracy. On the other hand the

extremely long time of calculation does not allow for mesh refinement to increase the accuracy. Global and average indicators show proper trend of convergence. However, the main disadvantage of this method, its slow rate of convergence, is still challenging for future research.

The results of the calculation can be summed up from various points of view, like accuracy, performance, ease in handling, portability. In Table 8 we present grades for each tested code with respect to accuracy, performance and ease in handling. For assessment of the accuracy we calculate grid convergence index (GCI) suggested by Roache [17] for uniform convergence reporting making use of data presented in Tables 3–6. Normalised computing time, based on the time of the calculation performed on Pentium 2.4 GHz PC computer for task with uniform mesh size  $100 \times 100$ , was used to assess the performance. Ease in handling was judged by our experience.

**Table 8** Comparison of computer codes from various points of views

	Accuracy		Performance (computing time)	Easiness in handling	
	GCI	Grade	Normalised	Grade	Grade
			time (sec)		
FRECON	0.002	A	1578	A	C
FLUENT	0.001	A	80000	B	A
FIDAP	0.025	B	6000	A	B
SOLVSTR	0.012	B	20000	A	C
SOLVMEF	0.042	C	2419000	D	C

A: very good; B: good; C: poor; D: unsatisfactory.

## 5 CONCLUSIONS

This paper proposes new reference solution for testing numerical codes dealing with the natural convection. The solution is obtained for very fine mesh and used for competition with four other codes. Nine velocity profiles are extracted and given in the form of high-order polynomials. The measure of performance of the solutions in question is investigated in terms of the standard deviation of the corresponding velocity profiles.

Two commercial codes based on finite volume approximation (Fluent) and finite element method (Fidap) are verified using the above method, along with a new mesh-free numerical approach as well as the classical finite difference approximation code. It appears that the defined measure of the code accuracy is very sensitive and detects very small deviation occurring in the velocity profiles. The precise analysis of defined convergence indicators allowed to judge that only Fluent solutions for the finest mesh is close enough to the reference solution. It is noteworthy that the Fluent solution was obtained on the mesh of  $380 \times 380$  nodes, almost twice as dense as the reference solution. All other solutions obtained for quite fine meshes are not sufficiently accurate, according to the defined measure. Successive mesh refinement is necessary to obtain a

satisfactory level of convergence, which on the other hand makes these calculations very slow and inevitably leads to the numerical diffusion due to the round-off errors.

The mesh-free calculation performed for the defined benchmark configuration turned out to be very time-consuming and slowly convergent. The same simulation using classical finite difference approach takes ten times less of the computational time. Of course due to the simple geometry we could not observe any advantages of mesh-free implementation. The aim of this comparison was solely verification of performance of the method applied to natural convection problem. Described diffuse approximation approach in mesh-free method turned out to perform extremely slow in comparison with the classical method. Future work is necessary to improve initial phase of this methodology, including application of randomly generated collocation points or its generation using predefined measure of sensitivity as well as application of more sophisticated solvers.

## ACKNOWLEDGEMENTS

This work was supported by Polish Scientific Committee (KBN Grant No. 8T09A00820). Some computations were conducted at the Interdisciplinary Centre of Mathematical and Computer Modelling, Warsaw University (ICM).

## REFERENCES

- 1 De Vahl Davis, G. (1983) 'Natural convection of air in a square cavity: a bench mark numerical solution', *Int. Journal for Numerical Methods in Fluids*, Vol. 3, No. 3, pp.249–264.
- 2 Banaszek, J., Jaluria, Y., Kowalewski, T.A. and Rebow, M. (1999) 'Semi-implicit FEM analysis of natural convection in freezing water', *Numerical Heat Transfer, Part A*, Vol. 36, No. 5, pp.449–472.
- 3 Kowalewski, T.A. and Rebow, M. (1999) 'Freezing of water in a differentially heated cubic cavity', *Int. J. Comp. Fluid Dyn.*, Vol. 11, Nos. 3–4, pp.193–210.
- 4 FLUENT 6 (2002) *User's Guide*, Fluent Inc. Lebanon, NH 2002.
- 5 FIDAP 8.7. (2002) *User's Guide*, Fluent Inc. Lebanon, NH 2002.
- 6 Leonardi, E., Kowalewski, T.A., Timchenko, V. and de Vahl Davis, G. (1999) 'Effects of finite wall conductivity on flow structures in natural convection', CHMT99, in Mohamad, A.A. and Sezai, I. (Eds.): *Proc. of Int. Conf. Comp. Heat and Mass Transfer*, Eastern Mediterranean University Printinghouse, Cyprus, pp.182–188.
- 7 Giangi, M., Stella, F. and Kowalewski, T.A. (1999) 'Phase change problems with free convection: fixed grid numerical simulation', *Comput Visual Sci.*, Vol. 2, Nos. 2–3, pp.123–130.
- 8 Giangi, M., Kowalewski, T.A., Stella, F. and Leonardi, E. (2000) 'Natural convection during ice formulation: numerical simulation vs. experimental results', *Computer Assisted Mechanics and Engineering Sciences*, Vol. 7, No. 3, pp.321–342.

9 Yeoh, G.H., Behnia, M., de Vahl Davis, G. and Leonardi, E. (1990) 'A numerical study of three-dimensional natural convection during freezing of water', *Int. J. Num. Meth. Eng.*, Vol. 30, No. 9, pp.899–914.

10 Mallinson, G.D. and de Vahl Davis, G. (1977) 'Three dimensional natural convection in a box: a numerical study', *J. Fluid Mech.*, Vol. 83, No. 1, pp.1–31.

11 Atluri, S.N. and Shen, S. (2002) *The Meshless Local Petrov-Galerkin (MLPG) Method*, Tech Science Press, Encino.

12 Liu, G.R. (2003) *Mesh-free Methods*, CRC Press, Boca Raton.

13 Sarler, B. (2002) 'Towards mesh-free computation of transport phenomena', *Engineering Analysis with Boundary Elements*, Vol. 26, No. 9, pp.731–738.

14 Kovacevic, I., Poredos, A. and Sarler, B. (2003) 'Solving the Stefan problem with the radial basis function collocation method', *Numerical Heat Transfer, Part B*, Vol. 44, No. 6, pp.577–599.

15 Prax, C., Salagnac, P. and Sadat, H. (1998) 'Diffuse approximation and control-volume-based finite-element methods: a comparative study', *Numerical Heat Transfer, Part B*, Vol. 34, No. 3, pp.303–321.

16 Sadat, H. and Couturier, S. (2000) 'Performance and accuracy of a meshless method for laminar natural convection', *Numerical Heat Transfer, Part B*, Vol. 37, No. 4, pp.455–467.

17 Roache, P.J. (1998) *Verification and Validation in Computational Science and Engineering*, Hermosa Publishers, Albuquerque, New Mexico 87119-9110 USA.

APPENDIX

**Table A1** The numerical values of the coefficients of polynomials describing profiles of the two velocity components and temperature for the selected benchmark solution (FRE6). The coefficients were obtained by nonlinear least-squares (NNLS) Marquardt-Levenberg algorithm. The order of polynomials was selected so that the remaining fit error (standard deviation relative to the maximum value) remained below 1%

	U	W	Temperature
<i>X = 0.5</i>			
a <sub>0</sub>	0.653255375988277	-0.0182133390825522	0.375731268271168
a <sub>1</sub>	-236.702203764653	-0.534506952806084	0.0646566206852292
a <sub>2</sub>	1443.71621734046	-4649.62374660758	-3.44261930694882
a <sub>3</sub>	-13999.9971459506	9166.34090898581	80.5716617494023
a <sub>4</sub>	-48978.2873061909	184756.318840003	-849.389178138508
A <sub>5</sub>	769502.177696391	-2267214.57474188	5426.31856180659
a <sub>6</sub>	-2826411.42861687	13921830.6389979	-20619.6870300723
a <sub>7</sub>	5049355.25968998	-50905496.7836152	47584.9389176856
a <sub>8</sub>	-4889309.49455426	117326421.048108	-66982.5680747791
a <sub>9</sub>	2473294.32955038	-175454949.94745	54146.8042661755
a <sub>10</sub>	-514661.642022168	170542299.447756	-18312.94874948
a <sub>11</sub>		-104264882.357183	-5638.00828334596
a <sub>12</sub>		36505160.4951902	6840.33395345218
a <sub>13</sub>		-5592440.58260601	-1672.49783568399
<i>Y = 0.5</i>			
a <sub>0</sub>	-0.971923736403444	1.00212115245059	0.999467521831559
a <sub>1</sub>	435.542611756185	12877.9988611009	-6.23069515529224
a <sub>2</sub>	-35897.4472988611	-259340.543848846	-18.9999577130502
a <sub>3</sub>	1124550.4608794	2053796.14649148	433.527770212382
a <sub>4</sub>	-19836290.5781327	-5602841.78532119	7318.66314332766
a <sub>5</sub>	217415780.824244	-30304885.3151783	-180265.707163689
a <sub>6</sub>	-1573770830.54861	358963997.276281	1714792.57838228
a <sub>7</sub>	7864305725.45593	-1697089432.98434	-9862261.15685317
a <sub>8</sub>	-27964717917.5742	4892293454.42925	38472869.7475459
a <sub>9</sub>	72090244360.2021	-9357882052.45715	-106665059.51901
a <sub>10</sub>	-135881981012.186	12081139841.5678	214297962.730994
a <sub>11</sub>	187042192305.203	-10321221406.5473	-313025047.586471
a <sub>12</sub>	-185722571203.416	5462280648.88341	328987879.084903
a <sub>13</sub>	129406337902.134	-1489621427.86707	-242193161.156869
a <sub>14</sub>	-59987319824.8771	62096039.6233113	118435075.266555
a <sub>15</sub>	16604163672.9515	43140732.9300454	-34530031.2923873
a <sub>16</sub>	-2075551754.938	0.321619021644532	4539519.05438302

**Table A1** The numerical values of the coefficients of polynomials describing profiles of the two velocity components and temperature for the selected benchmark solution (FRE6). The coefficients were obtained by nonlinear least-squares (NLS) Marquardt-Levenberg algorithm. The order of polynomials was selected so that the remaining fit error (standard deviation relative to the maximum value) remained below 1% (continued)

	<i>U</i>	<i>W</i>	Temperature
<i>X</i> = 0.9			
<i>a</i> <sub>0</sub>	1.37834316239398	1.11560341761746	0.308900034946171
<i>a</i> <sub>1</sub>	869.803859921856	-682.103162659822	-0.574121199057708
<i>a</i> <sub>2</sub>	74379.0946531731	64546.3444091368	74.382226060503
<i>a</i> <sub>3</sub>	-3924258.51426546	-2657731.00888943	-3161.22612928187
<i>a</i> <sub>4</sub>	89435741.7003693	60098287.7693382	74817.9579968359
<i>a</i> <sub>5</sub>	-1217186200.6406	-822661490.080435	-1125745.01070913
<i>a</i> <sub>6</sub>	10971526417.6405	7425487150.03986	11435967.2156945
<i>a</i> <sub>7</sub>	-69219909243.1401	-46729243229.224	-81662746.1201518
<i>a</i> <sub>8</sub>	316473663407.374	212583413470.936	421890116.068198
<i>a</i> <sub>9</sub>	-1072529330832.37	-715751344227.008	-1608940868.43137
<i>a</i> <sub>10</sub>	2732146343933.84	1809508968294.41	4588612041.2787
<i>a</i> <sub>11</sub>	-5267137304120.64	-3459353036180.82	-9850623665.12099
<i>a</i> <sub>12</sub>	7684697385210.4	5001906037363.17	15919604870.6355
<i>a</i> <sub>13</sub>	-8422179003474.85	-5429815720822.07	-19229337194.963
<i>a</i> <sub>14</sub>	6816871501820.86	4350956298121.35	17073562106.7329
<i>a</i> <sub>15</sub>	-3949555692631.44	-2494534120078.54	-10804649895.8457
<i>a</i> <sub>16</sub>	1548473261831.82	967384927672.173	4608652340.13695
<i>a</i> <sub>17</sub>	-367847357872.57	-227214939183.605	-1186818611.97188
<i>a</i> <sub>18</sub>	39966515019.2774	24398428716.3919	139329555.368117